COMPUTATIONAL THERMAL SCIENCES: *AN INTERNATIONAL JOURNAL*

ASTFE

An Official Journal of the American Society of Thermal and Fluids Engineers

Publisher: Begell House, USA.

ISSN Print: 1940-2503; ISSN Online: 1940-2554

Accepted May 26th 2020

COMPUTATION OF EYRING-POWELL MICROPOLAR CONVECTIVE BOUNDARY LAYER FLOW FROM AN INVERTED NON-ISOTHERMAL CONE: *THERMAL POLYMER COATING SIMULATION*

S. A. Gaffar[1], O. Anwar Bég[2], V. R. Prasad [3], B. M. H. Khan[4] and Ali Kadir[2]*

[1] Department of Mathematics, Salalah College of Technology, Salalah, ***Oman***

[2] Aeronautical/Mechanical Engineering Division, University of Salford, M5 4WT, ***UK***

[3] Department of Mathematics, School of Advanced Science, VIT University, Vellore, ***India***

[4]Department of Mathematics, Sir Vishveshwaraiah Institute of Science and Technology, Madanapalle, ***India***

***Corresponding Author Email:** abdulsgaffar0905@gmail.com*

ABSTRACT

Thermal coating of components with non-Newtonian materials is a rich area of chemical and process mechanical engineering. Many different rheological characteristics can be simulated for such coatings with a variety of different mathematical models. In this work we study the steady-state coating flow and heat transfer of a non-Newtonian liquid (polymer) on an inverted isothermal cone with variable wall temperature. The Eringen micropolar and three-parameter Eyring-Powell models are combined to simulate microstructural and shear characteristics of the polymer. The governing partial differential conservation equations and wall and free stream boundary conditions are rendered into dimensionless form and solved computationally with the Keller-Box finite difference method (FDM). Validation with earlier Newtonian solutions from the literature is also included. Graphical and tabulated results are presented to study the variations of fluid velocity, micro-rotation (angular velocity), temperature, skin friction, wall couple stress (micro-rotation gradient) and wall heat transfer rate. With increasing values of the first Eyring-Powell parameter temperatures are elevated, micro-rotation is suppressed and velocities are enhanced near the cone surface but reduced further into the boundary layer. Increasing values of the second Eyring-Powell parameter induce strong flow deceleration, decrease temperatures but enhance micro-rotation values. An increase in non-isothermal power law index suppresses velocities, temperatures and micro-rotations i.e. all transport characteristics are maximum for the isothermal case (n =0). Increasing Eringen vortex viscosity parameter significantly enhances temperatures and also micro-rotations. The present numerical simulations find applications in thermal polymer coating operations and industrial deposition techniques and provide a useful benchmark for more general computational fluid dynamics (CFD) simulations.

KEYWORDS: *Eyring-Powell model; Micropolar fluid; vortex viscosity; wall couple stress; angular velocity; heat transfer rate; thermal polymer coating; cone; computational.*

1.INTRODUCTION

Polymer coating processes often feature heat transfer. Numerous heat sensitive polymeric materials are required for deposition on a broad range of substrates and mechanical components. They provide important engineering enhancement features in numerous areas of technology including corrosion protection [1] and arise in also in adhesion manufacture [2], optical fiber enrobing [3], minimization of surface defects [4] and plastic surfacing [5]. Generally, the polymeric liquids employed in coating exhibit non-Newtonian characteristics and different coating techniques are needed for different fluids [6]. Pre-metered coating techniques (including slot die technology) contract and expand the fluid whereas roll coating divides the coating film as rotational forces interact with surface tension forces. Many rheological models have been developed to simulate the diverse characteristics of polymeric coatings and are lucidly reviewed by Tanner [7]. They include rheopetic fluids (which show a transient variation in viscosity and thicken or solidify when agitated), viscoplastic liquids (requiring a yield stress to initiate flow), simple and complex viscoelastic fluids, power-law liquids, microstructural liquids etc. Viscoelastic fluids exhibit both viscous behaviour and elastic deformation and arise in many coating systems including waterborne acrylic polymer/silica nanocomposites [8], heat-dissipating hybrid liquids [9] and rotor blade surface finishes [10]. When The hot melt adhesive polymer experiences stresses for a short time, the viscoelasticity is considered linear and slow deformations of the molecules occur. A number of different rheological models have been implemented to simulate coating heat transfer including Phan-Thein-Tanner fluids [11], pseudoplastic/dilatant fluids [12], Casson viscoplastic nanofluids [13], second order Reiner-Rivlin elastic-viscous liquids [14] and exponential viscosity models [15]. A relatively simple but useful non-Newtonian model is the Eyring-Powell model [16] which is derived from the kinetic theory of liquids rather than the empirical relations. It allows Newtonian behavior to be extracted as a special case for low and high shear stress scenarios. This model is a modification of the Powell model which has also been shown (at moderate stresses) to exhibit exponential dependence of the flow velocity on the stress, but a linear dependence at higher stresses. This model has been employed successfully in simulating stretching sheet coating flows in recent years and relevant studies include Khan *et al.* [17] (on reactive polymer stretching flow) and Ibrahim and Gadisa [18] (on finite element simulation of nano-doped Eyring-Powell fluids from extending surfaces). Yoon and Ghajar [19] showed that Powell-Eyring fluid is highly sensitive to the small variations in the zero-shear rate viscosity and moderately sensitive to the changes in the infinite shear rate viscosity. Other studies featuring this model include Alharbi et al. [20] (on

magnetic polymer entropy generation), Malik *et al.* [21] (on mixed convection of magnetized Eyring-Powell fluids), Sirohi *et al.* [22], Rahimi *et al.* [23], Hina *et al.* [24] and Khan *et al.* [25]. All these studies have confirmed the deviation of fluid/thermal characteristics of Eyring-Powell fluids from Newtonian fluids. While certain features of polymer fluids can be captured quite well with the Eyring-Powell model, it does not provide a robust framework for micro-structural characteristics associated with suspensions present in many coatings. Many polymeric and industrial fluids (propellants, gels, coolants, coatings etc) exist which possess a complex micro-structure that effectively contributes strongly to their performance characteristics. Eringen [26] developed *micro-morphic fluid mechanics as a framework for simulating micro-structural rheological* effects for suspensions containing deformable particles and featuring micro-rotation (spin) and micro-inertia. Eringen further derived the micropolar fluid model [27] as a special case of micro-morphic fluids with non-deformable micro-elements. The micropolar model is much simpler than micromorphic fluids since that it reduces the original eighteen balance equations to a maximum of six momenta balance equations (three for linear and three for angular). Also it allows the extraction of the Navier-Stokes classical viscous model as a very special case when micro-polar effects are negated. Micropolar fluids are therefore a special case of general micromorphic fluids with non-symmetric stress tensor. Micropolar fluids physically consist of arbitrarily oriented rigid particles suspended in viscous medium. In [28] Eringen generalized micropolar fluids to consider heat conduction and thermophysics. The elegant formulation provided for micropolar fluids has made this model very popular in boundary layer flows which are relevant to coating applications. It has been employed in surface tension-driven systems [29], anti-fouling bacterial coating flows [30], slip dynamics in magnetic materials processing [31], simulation of chemical reactions in polymer extrusion flows [32], thermal convection flows from contracting sheets [33] and unsteady micropolar nanoliquid flows containing suspended micro-organisms for bio-polymer synthesis. These studies have all shown that the Eringen vortex viscosity and micropolar rheological parameters considerably modify the velocity and temperature characteristics in coating systems in addition to furnishing important information on the spin characteristics of the microelements.

As noted earlier, heat transfer analysis is central to thermal polymer processing. Here the wall may be constant temperature (isothermal) or non-isothermal (variable temperature from the slit to the downstream location). The latter is more appropriate for real systems [5-7] and extensive studies have been conducted to evaluate the impact of non-isothermal wall conditions on flow dynamics. Relevant works include Sobhani *et al.* [35] who used a

Galerkin computational method to analyse on non-isothermal rheological extrusion with viscous dissipation. Li *et al.* [36] employed an adaptive coupled finite element (FE) and meshfree (MF) approach to examine non-isothermal injection viscoelastic molding processes. Debbaut [37] investigated the non-isothermal squeeze flow of viscoelastic fluids, also considering boundary layer structures. Reddy *et al*. [38] studied the unsteady non-isothermal flow and heat transfer with entropy generation in a polymer using the second order Reiner-Rivlin model and a Crank-Nicholson difference method. Reisfeld and Bankoff [39] investigated non-isothermal flow of a viscous liquid film on the surface of a heated or cooled cylinder with gravity, capillary, thermocapillary, and intermolecular forces. Gaffar *et al.* [40] computed the velocity and temperature fields for electrically conducting viscoelastic polymer from a non-isothermal wedge with convective boundary conditions. Further studies include Cheung [41] (on "freeze coating" on a moving non-isothermal plate), Rashidi *et al.* [42] (on third grade viscoelastic non-isothermal Falkner-Skan flow), Kuruneru et al. [43] (on unsteady heat transfer in metal foams), Bég *et al.* [44] (on surface-tension driven non-isothermal magnetic nanopolymer coating flows) and Nepershin [45] (on non-isothermal plastic flow).

In the present study we combine the Eyring-Powell model and Eringen micropolar model to study viscoelastic micropolar boundary layer coating flow from a vertical cone with variable wall temperature. The governing conservation equations for mass, linear momentum, angular momentum and energy (heat) with associated boundary conditions are transformed to non-dimensional coupled partial differential boundary value problem. The nonlinearity of the emerging model does not permit exact solutions and therefore an implicit finite difference computational method (Keller's box method) [46] is utilized. Linear velocity, micro-rotation (angular velocity of micro-elements), temperature, skin friction, Nusselt number (wall heat transfer rate) and wall couple stress (micro-rotation gradient) are computed for different values of the Eyring-Powell rheological parameters, Eringen vortex viscosity parameter, Prandtl number, streamwise coordinate and non-isothermal parameter (surface power-law exponent). Validation of the Keller box solutions is conducted with earlier Newtonian studies [47]. The simulations are relevant to thermal coating systems in chemical engineering.

2.MATHEMATICAL MODEL

The laminar, steady-state, incompressible, thermal convection flow of an *Eyring-Powell micropolar fluid* from an inverted isothermal cone with variable wall temperature (non-isothermal) is studied, as illustrated in **Fig. 1**. Both the fluid and cone are initially

maintained at constant temperature. The (x, y) coordinates are measured along and normal to the cone surface with the vertex placed at the origin.

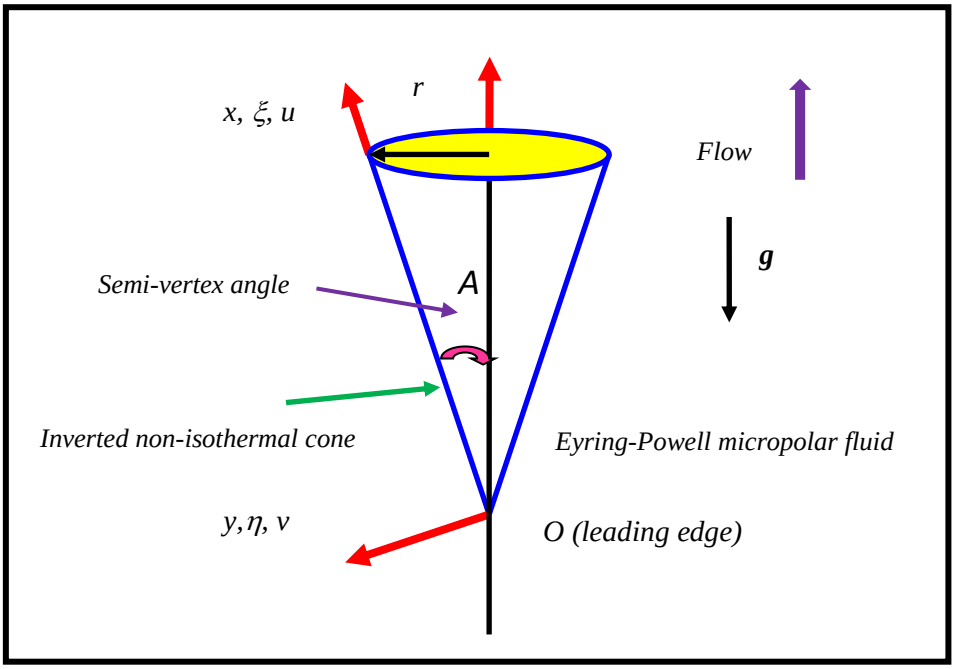

Fig. 1 Geometric illustration of problem

Further, $r(x) = x\sin A$ is the radius of the cone with A being the half angle of the cone. The cone surface is non-isothermal i.e. it has variable temperature such that $T_w(x) = T_\infty + d_1 x^n$, is higher than the ambient fluid temperature T_∞ and where d_1 is a constant and n is the surface temperature exponent. Moreover, under the usual boundary layer and Boussineq approximations, the relevant equations may be presented as the mass, linear momentum, angular momentum and energy conservation equations:

$$\frac{\partial(ru)}{\partial x} + \frac{\partial(rv)}{\partial y} = 0 \tag{1}$$

$$u\frac{\partial u}{\partial x} + v\frac{\partial u}{\partial y} = \left(\nu + \frac{k}{\mu} + \frac{1}{\rho\beta_1 C_1}\right)\frac{\partial^2 u}{\partial y^2} - \frac{1}{2\rho\beta C^3}\left(\frac{\partial u}{\partial y}\right)^2\frac{\partial^2 u}{\partial y^2} + g_1\beta_1(T - T_\infty)\cos A + k\frac{\partial N}{\partial y} \tag{2}$$

$$\rho j\left(u\frac{\partial N}{\partial x} + v\frac{\partial N}{\partial y}\right) = \gamma\frac{\partial^2 N}{\partial y^2} - k\left(2N + \frac{\partial u}{\partial y}\right) \tag{3}$$

$$u\frac{\partial T}{\partial x} + v\frac{\partial T}{\partial y} = \alpha\frac{\partial^2 T}{\partial y^2} \tag{4}$$

The associated boundary conditions on the cone surface (wall) and in the free stream (edge of the boundary layer) are:

$$\text{At} \quad y = 0,\ u = 0,\ N = -\frac{1}{2}\frac{\partial u}{\partial y},\ T_w(x) = T_\infty + d_1 x^n$$

$$\text{As} \quad y \to \infty,\ u \to 0,\ N \to 0, \qquad T \to T_\infty \tag{5}$$

Here u and v are the velocity components in the x and y directions respectively, ν is the kinematic viscosity, ρ is the density of the fluid, g_1 is gravitational acceleration, k is the vortex viscosity, β and C are Eyring-Powell non-Newtonian parameters, β_1 is the coefficient of thermal expansion, N is the angular velocity, j is the micro-inertia per unit mass, $\gamma^* = \left(\mu + \frac{k}{2}\right) j$ is the gyro-viscosity (shear spin) of micropolar, α is the thermal diffusivity, T is the temperature of the fluid, T_∞ is the free stream temperature. Eqn. (1) is automatically satisfied subject to the velocity components expressed in terms of stream function as $ru = \frac{\partial \psi}{\partial y}$ *and* $rv = -\frac{\partial \psi}{\partial x}$.

The following non-dimensional quantities are introduced:

$$\xi = \frac{V_w x}{v} Gr_x^{-\frac{1}{4}}, \eta = \frac{y}{x} Gr_x^{\frac{1}{4}}, \psi = rv\sqrt[4]{Gr_x}\left(f + \frac{1}{2}\xi\right), \theta(\xi,\eta) = \frac{T - T_\infty}{T_w - T_\infty}, Pr = \frac{v}{\alpha}$$

$$g = \frac{x^2 N}{v} Gr^{-\frac{3}{4}}, Gr_x = \frac{g\beta(T_w - T_\infty)x^3 \cos A}{4V^2}, \varepsilon = \frac{1}{\mu\beta C}, \delta = \frac{V^2}{2C^2x^2} Gr_x^{\frac{3}{2}}, K = \frac{k}{\mu} \tag{6}$$

Here ξ and η are the dimensionless tangential and radial coordinates respectively, Gr_x is the *local Grashof number*, ψ is stream function, θ is the *non-dimensional temperature*, *Pr* is the *Prandtl number*, g is the *dimensionless angular velocity (micro-rotation)*, ε is the Eyring-Powell *rheological fluid parameter*, δ is the local *non-Newtonian parameter and K* is the Eringen *vortex viscosity parameter*. Eqns. (2)-(5) are thereby rendered into the following coupled nonlinear partial differential boundary layer equations:

Linear Momentum

$$(1+K+\varepsilon) f''' + \frac{n+7}{4} ff'' + Kg' - \frac{n+1}{2} f'^2 + \xi f'' - \varepsilon\delta (f'')^2 f''' + \theta = \frac{1-n}{4}\xi\left(f'\frac{\partial f'}{\partial \xi} - f''\frac{\partial f}{\partial \xi}\right) \tag{7}$$

Angular Momentum (Micro-rotation)

$$\left(1+\frac{K}{2}\right) g'' - BK\xi^2 [2g + f''] + \frac{n+7}{4} fg' - \frac{1+3n}{4} f'g + \xi g' = \frac{1-n}{4}\xi\left(f'\frac{\partial g}{\partial \xi} - g'\frac{\partial f}{\partial \xi}\right) \tag{8}$$

Energy

$$\frac{\theta''}{\Pr}+\frac{n+7}{4}f\theta'-n\theta f'+\xi\theta'=\frac{1-n}{4}\xi\left(f'\frac{\partial\theta}{\partial\xi}-\theta'\frac{\partial f}{\partial\xi}\right) \tag{9}$$

with:

$$\begin{aligned} &At \quad \eta=0, \quad f=0, \quad f'=0, \quad g=\frac{1}{2}\frac{\partial^2 f}{\partial y^2}, \quad \theta=1 \\ &As \quad \eta\to\infty, \quad f'\to 0, \quad g\to 0, \quad \theta\to 0 \end{aligned} \tag{10}$$

Here primes denote the differentiation with respect to η and $B=\frac{\nu^2}{jV_w}$ is the micro-inertia density (micropolar material) parameter. The *skin-friction coefficient (C_f) (shear stress at the cone surface), Wall Couple Stress (Wcs) and Nusselt number (Nu) (heat transfer rate)* are defined using the following expressions.

$$Gr_x^{-3/4}C_f=\left(1+\frac{K}{2}+\varepsilon\right)f''(\xi,0)-\frac{\delta}{3}\varepsilon\left(f''(\xi,0)\right)^3 \tag{11}$$

$$M_w=g'(\xi,0) \tag{12}$$

$$Gr_x^{-1/4}Nu=-\theta'(\xi,0) \tag{13}$$

3. KELLER BOX IMPLICIT SCHEME SOLUTIONS AND VALIDATION

The dimensionless Eqns. (7) – (9) along with boundary conditions, Eqn. (10) is a 7th order non-linear coupled boundary value problem requiring a numerical solution. The implicit finite difference scheme known as the Keller-Box method (KBM) [46] is implemented to solve the system of Eqs. (7) – (10). This technique is very popular and most efficient as compared to other numerical techniques. With a second order accuracy, the KBM is very stable and rapidly convergent. KBM comprises of the following 4 steps:

(i)Reduction of Nth order partial differential system to N first order differential equations.

(ii)Finite difference discretization.

(iii)Newton quasilinearization of non-linear Keller algebraic equations.

(iv)Block-Tridiagonal elimination of Keller algebraic equations.

KBM has been used extensively in recent years in many nonlinear fluid dynamic problems including radiative magnetized non-Newtonian coating flow on a cone [48], variable viscosity flow on a cylinder [49], tangent hyperbolic fluid coating heat transfer [50], metallic

nanofluid stretching sheet flow [51], oxytactic nano-bioconvection fuel cells [52], magnetized micropolar buoyancy-driven flow [53] fractional subdiffusion equations in applied mechanics [54]. Algebraic discretization details are omitted here for brevity. The reader is referred to [46]-[52] for more details. To validate the current KBM code, benchmarking with earlier Newtonian simulations has been conducted. **Table 1** presents the comparison values of *heat transfer rate*, *Nu*, for different values of ξ. The present results are compared with the Newtonian study of Hossain and Paul [47] and we found an excellent correlation which confirms the accuracy of the present Keller box computational method. Increasing streamwise coordinate, ξ, clearly leads to a reduction in Nusselt number indicating that with further distance from the apex, heat transfer rate is suppressed. The test case for Pr = 0.1 corresponds to very high thermal conductivity liquid and this inevitably elevates temperatures in the boundary layer and reduces heat transfer rate to the cone surface (wall), as noted in many studies including Incropera and De Witt [55]. Since non-isothermal flow is also considered (n = 0.5) this will also contribute to a depletion in wall heat transfer rates with progression along the cone surface from the vertex (ξ=0) to higher values of ξ.

Table 1: Comparison values of *Nu* for various values of ξ with n = 0.5, Pr = 0.1, ε = 0.0, δ = 0.0, K = B = 0.0

ξ	*Nu*	
	Hossain and Paul [47]	KBM
0.0	0.24584	0.2461
0.1	0.25089	0.2509
0.2	0.25601	0.2558
0.4	0.26630	0.2660
0.6	0.27662	0.2765
0.8	0.28694	0.2868
1.0	0.29731	0.2972
2.0	0.35131	0.3512

4. NUMERICAL RESULTS AND INTERPRETATION

The solutions generated with KBM are presented both numerically and graphically. Solutions for *skin friction (C_f), wall couple stress (Wcs) and heat transfer rate (Nu)* at the

cone surface are presented in **Tables 2 – 3**. The default values for the parameters involved in this analysis are taken as $\delta = 0.3 = \varepsilon$, $Pr = 0.71$, $\xi = 1.0$, $n = 0.5$, $B = 1.0$ and $K = 3.0$. *Further*, (ξ, η), are independent spatial variables. **Table 2** presents the values of C_f, *Wcs* and *Nu* for different values of *surface temperature exponent n*, *vortex viscosity*, *K* and streamwise coordinate, ξ.

Table 2: Values of C_f , *Nu* and *Wcs* for different values of *K*, *n* and ξ (Pr = 0.71, ε = 0.3 = δ, B = 0.5)

n	*K*	$\xi = 0.0$			$\xi = 1.0$			$\xi = 2.0$		
		C_f	*Nu*	*Wcs*	C_f	*Nu*	*Wcs*	C_f	*Nu*	*Wcs*
0.0	3.0	1.2070	0.3523	-0.0015	0.9026	0.8365	-0.0571	0.6062	1.4726	-0.0952
0.12		1.1873	0.3653	-0.0014	0.8907	0.8452	-0.0558	0.6025	1.4763	-0.0940
0.24		1.1692	0.3774	-0.0014	0.8795	0.8532	-0.0547	0.5987	1.4799	-0.0933
0.35		1.1537	0.3878	-0.0014	0.8700	0.8601	-0.0537	0.5953	1.4832	-0.0928
0.5		1.1341	0.4010	-0.0013	0.8580	0.8688	-0.0524	0.5915	1.4873	-0.0913
0.62		1.1195	0.4110	-0.0013	0.8491	0.8751	-0.0513	0.5883	1.4907	-0.0903
0.5	0.1	0.6911	0.4996	-0.0002	0.6265	0.9378	-0.0039	0.4799	1.5160	-0.0061
	0.25	0.7309	0.4906	-0.0003	0.6512	0.9312	-0.0105	0.4942	1.5129	-0.0215
	0.5	0.7893	0.4775	-0.0006	0.6864	0.9215	-0.0212	0.5136	1.5085	-0.0470
	0.75	0.8403	0.4661	-0.0006	0.7157	0.9132	-0.0301	0.5288	1.5049	-0.0644
	1.0	0.8855	0.4561	-0.0009	0.7406	0.9060	-0.0369	0.5410	1.5018	-0.0704
	1.5	0.9632	0.4388	-0.0011	0.7806	0.8939	-0.0457	0.5596	1.4969	-0.0890

Table 3: Values of C_f , *Nu* and *Wcs* for different values of ε, δ and *Pr*
(n = 0.5, K = 3.0, B = 0.5)

ε	δ	*Pr*	$\xi = 0.0$			$\xi = 1.0$			$\xi = 2.0$		
			C_f	*Nu*	*Wcs*	C_f	*Nu*	*Wcs*	C_f	*Nu*	*Wcs*
0.0	0.3	0.71	1.1941	0.4072	-0.0014	0.9142	0.8735	-0.0546	0.6343	1.4892	-0.0963
0.18			1.1572	0.4035	-0.0014	0.8796	0.8706	-0.0533	0.6080	1.4880	-0.0931
0.35			1.1247	0.4000	-0.0013	0.8493	0.8680	-0.0520	0.5849	1.4870	-0.0906

0.5			1.0977	0.3971	-0.0013	0.8243	0.8658	-0.0510	0.5661	1.4861	-0.0880
0.85			1.0574	0.3925	-0.0013	0.7873	0.8625	-0.0494	0.5380	1.4849	-0.0848
1.0			1.0174	0.3878	-0.0013	0.7509	0.8590	-0.0477	0.5106	1.4836	-0.0811
0.3	0	0.71	1.1335	0.4010	-0.0013	0.8577	0.8688	-0.0524	0.5914	1.4873	-0.0913
	5		1.1427	0.4015	-0.0014	0.8620	0..8689	-0.0525	0.5929	1.4873	-0.0914
	20		1.1734	0.4029	-0.0014	0.8758	0.8694	-0.0528	0.5982	1.4873	-0.0919
	40		1.2253	0.4051	-0.0014	0.8966	0.8702	-0.0532	0.6038	1.4875	-0.0923
	50		1.2587	0.4063	-0.0014	0.9085	0.8706	-0.0533	0.6071	1.4875	-0.0925
	80		1.4532	0.4113	-0.0014	0.9514	0.8718	-0.0540	0.6180	1.4876	-0.0932
0.3	0.3	0.5	0.6113	0.5180	-0.0004	0.5653	0.8146	-0.0197	0.5093	1.1845	-0.0602
		1.0	0.6044	0.5353	-0.0004	0.4785	1.2066	-0.0151	0.3623	2.0916	-0.0359
		2.0	0,5916	0.5675	-0.0004	0.3446	2.1346	-0.0087	0.2101	4.1060	-0.0142
		3.0	0.5800	0.5972	-0.0003	0.2611	3.1472	-0.0052	0.1473	6.1586	-0.0072
		5.0	0.5597	0.6504	-0.0003	0.1801	5.2798	-0.0022	0.1014	10.2617	-0.0027
		7.0	0.5424	0.6970	-0.0003	0.1489	7.2911	-0.0011	0.0901	14.3484	-0.0013

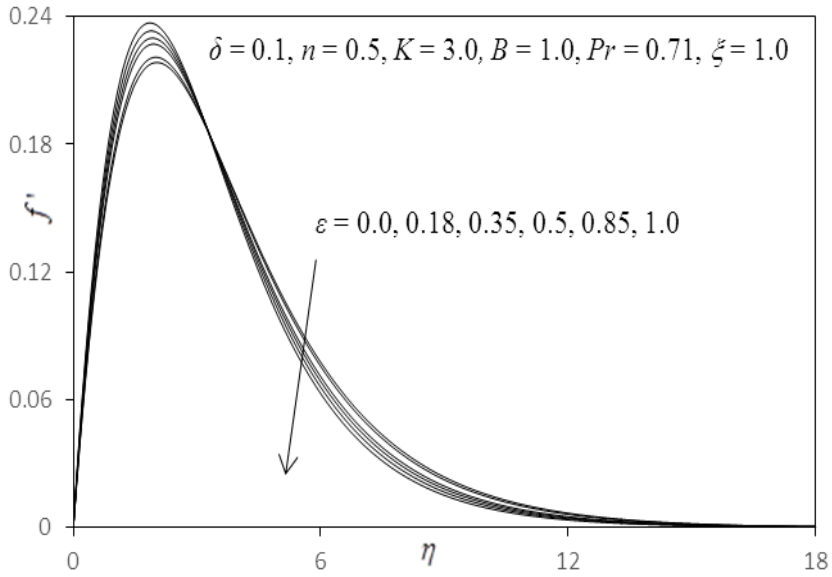

Fig. 2(a) Influence of ε on Velocity Profiles

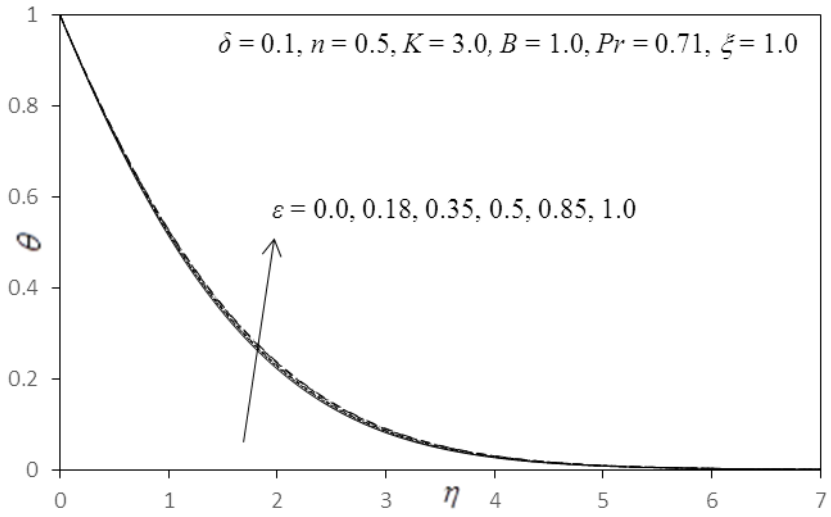

Fig. 2(b) Influence of ε on Temperature Profiles

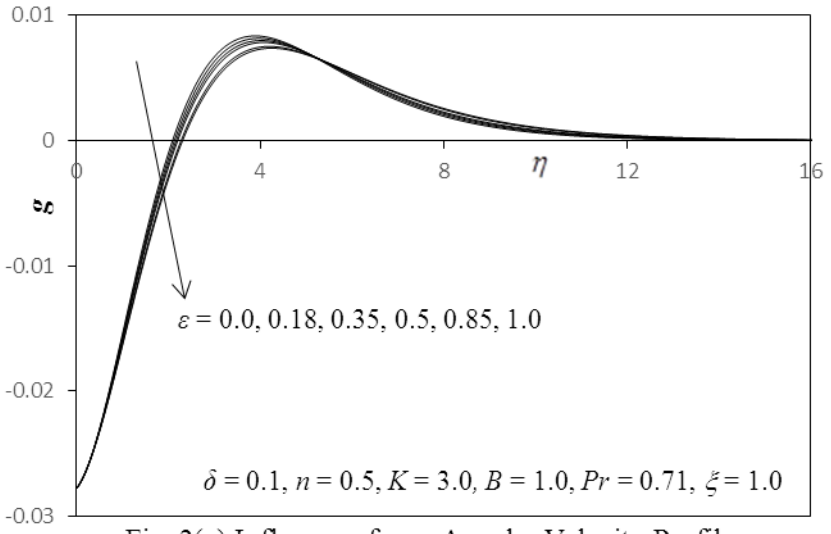

Fig. 2(c) Influence of ε on Angular Velocity Profiles

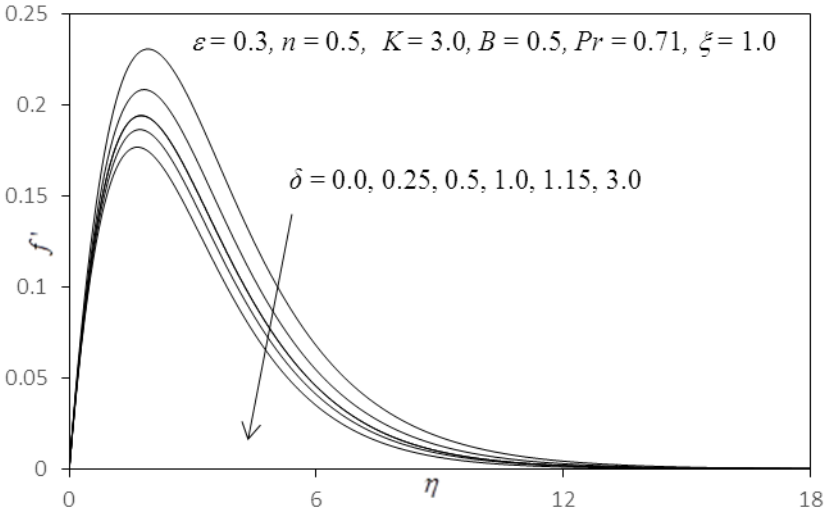

Fig. 3(a) Influence of δ on Velocity Profiles

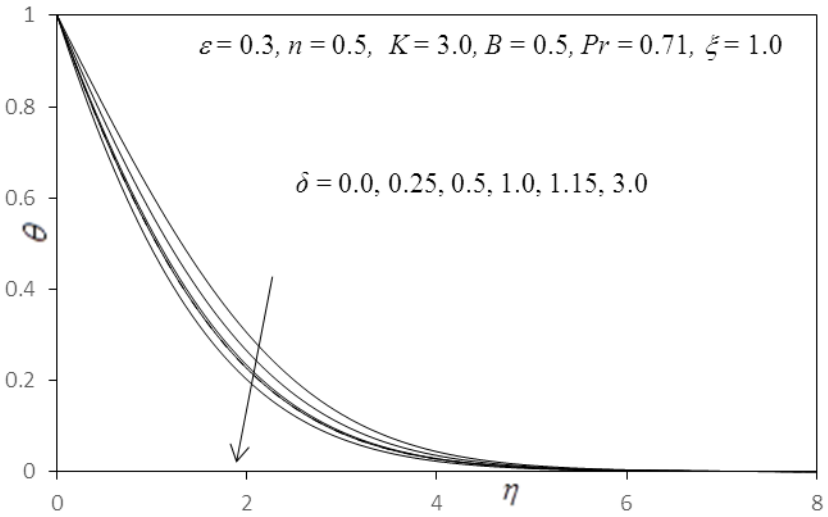

Fig. 3(b) Influence of δ on Temperature Profiles

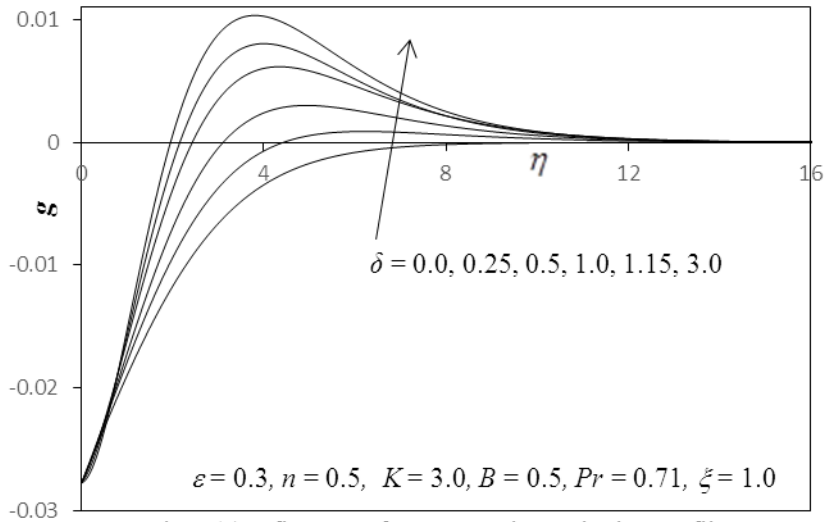

Fig. 3(c) Influence of δ on Angular Velocity Profiles

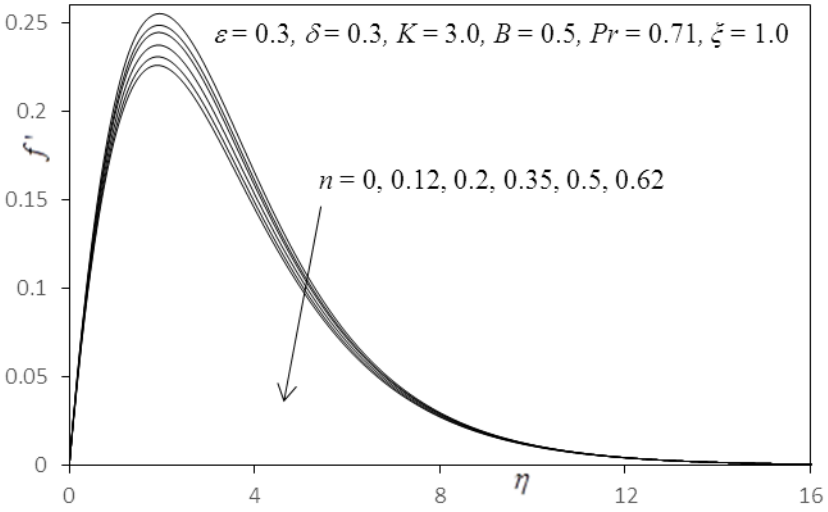

Fig. 4(a) Influence of n on Velocity Profiles

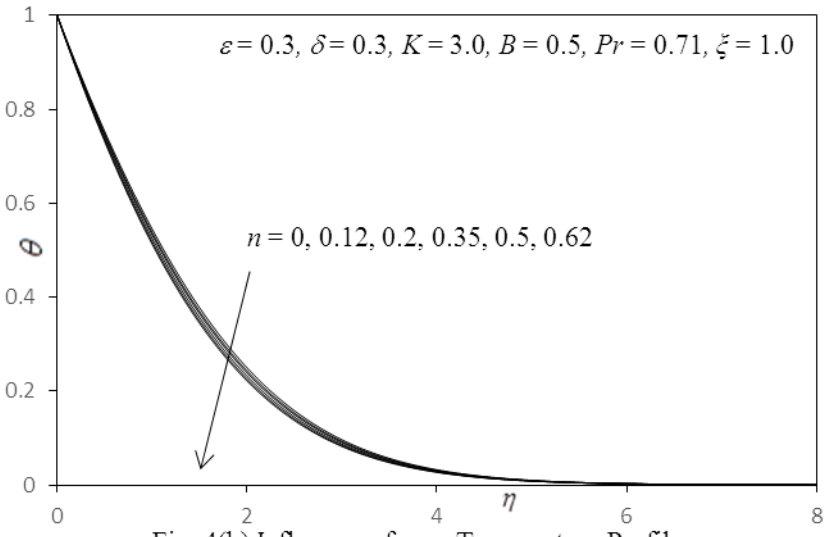

Fig. 4(b) Influence of n on Temperature Profiles

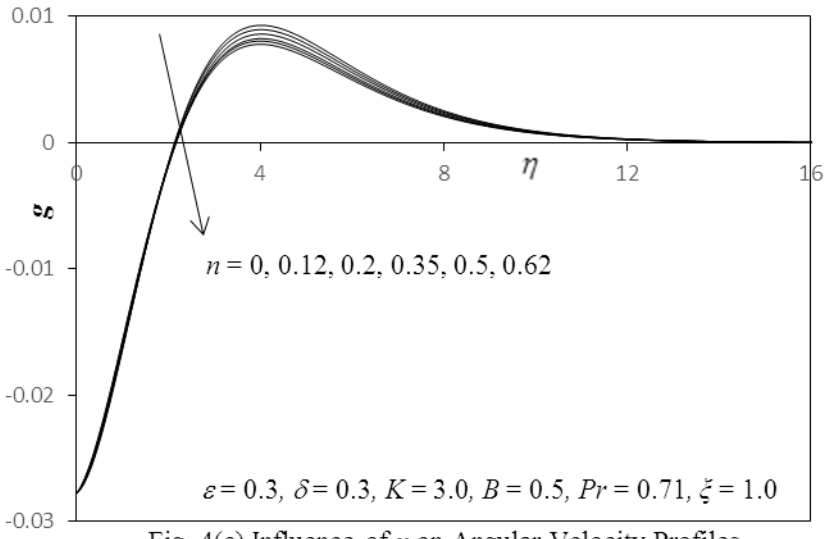

Fig. 4(c) Influence of n on Angular Velocity Profiles

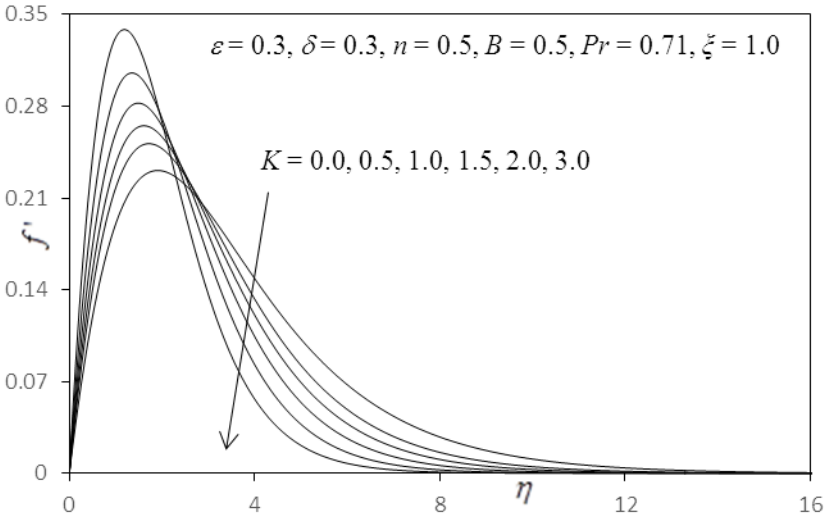

Fig. 5(a) Influence of K on Velocity Profiles

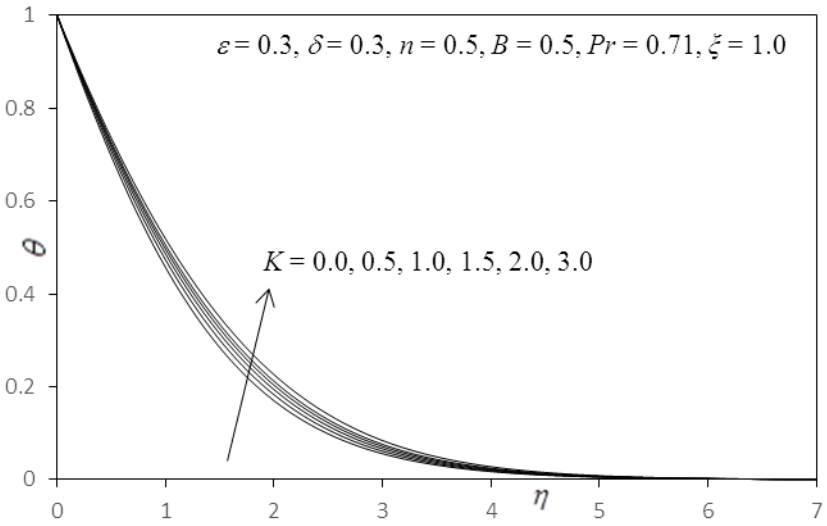

Fig. 5(b) Influence of K on Temperature Profiles

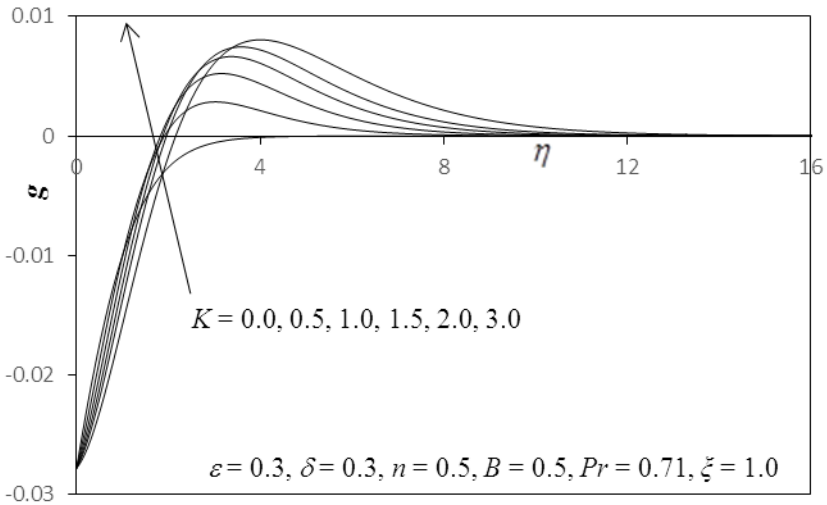

Fig. 5(c) Influence of K on Angular Velocity Profiles

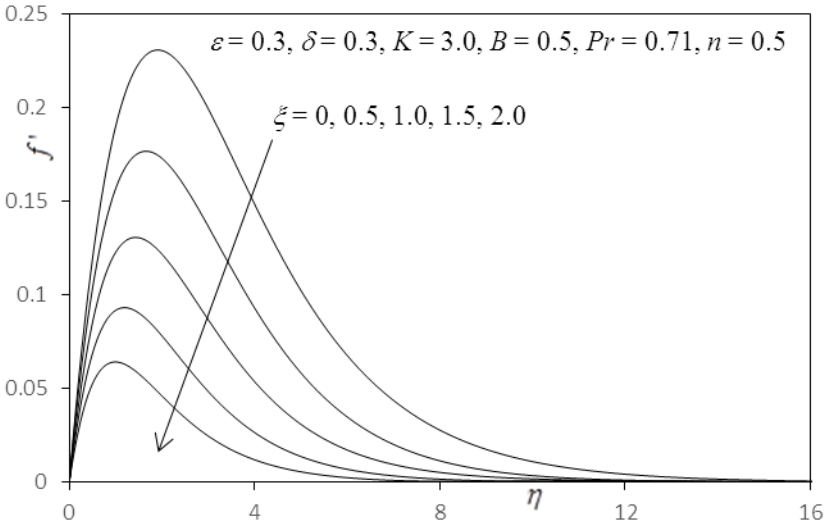

Fig. 6(a) Influence of ξ on Velocity Profiles

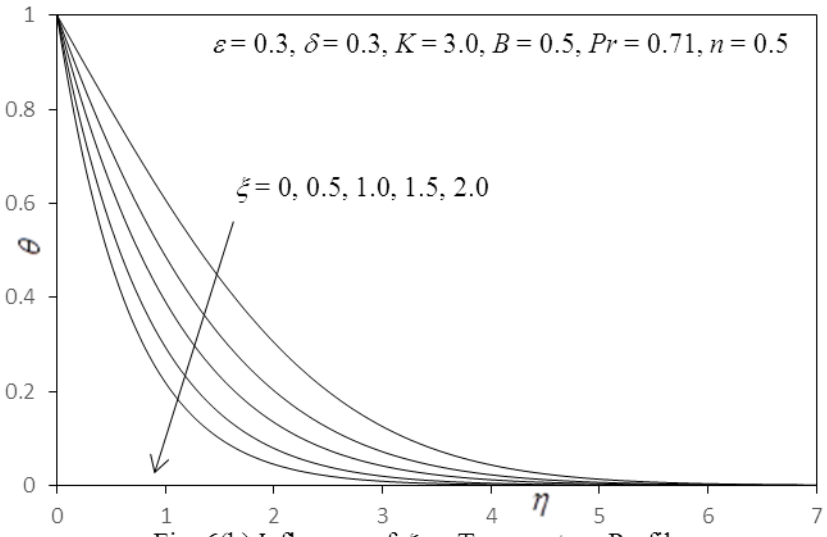

Fig. 6(b) Influence of ξ on Temperature Profiles

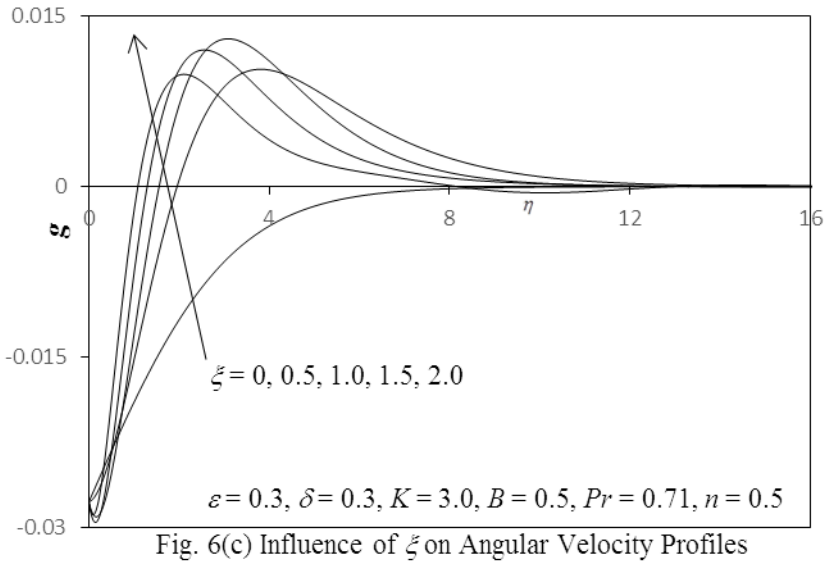

Fig. 6(c) Influence of ξ on Angular Velocity Profiles

An enhancement in surface temperature exponent, *n* clearly reduces skin friction, Nusselt number and wall couple stress i.e. C_f, *Nu and Wcs.* In Eqn. (5), $T_w(x) = T_\infty + d_1 x^n$ and clearly with $n>0$) the wall temperature is elevated. This increases heat transfer from the wall to the fluid and naturally suppresses heat transfer from the fluid to the wall. Via coupling with the momentum field and micro-rotation field, there is therefore a deceleration in the flow (decreasing skin friction)) and stifling of the rotary motions of micro-elements at the wall (decreasing wall couple stress i.e. micro-rotation gradient). The implication of using a non-isothermal model is therefore that wall quantities are more accurately predicted since the isothermal case (n=0) over-predicts them. An elevation in Eringen vortex viscosity parameter ($K = \frac{k}{\mu}$), however enhances skin friction, C_f, and wall couple stress, *Wcs* whereas it depletes

the Nusselt number, *Nu*. The flow is therefore accelerated, and rotation of the micro-elements is boosted with greater vortex viscosity effect. Strongly micropolar polymers (K>0.1) significantly benefits the boundary layer flow characteristics for linear and angular momentum and is also advantageous in terms of reducing heat transfer rates to the wall i.e. cooling the cone surface. This is of significance in temperature regulation in practical polymer coating operations since adversely high heat transfer rates at the wall may induce defects, thermal damage, de-bonding etc [6]. Increasing streamwise coordinate, ξ, induces a substantial retardation in the flow i.e. decreases skin friction. However, with higher streamwise coordinate values there is a marked elevation in Nusselt number (heat transfer rate to the wall is promoted) and also magnitudes of wall couple stress are enhanced (stronger spin in micro-elements is mobilized). The trends concur with other studies including Siddiqa *et al*. [54]. **Table 3** depicts the influence of ε, δ and *Pr* on C_f, *Wcs* and *Nu* in addition to streamwise coordinate, ξ. An increase in the first Eyring-Powell fluid parameter, ε, decreases C_f and *Nu* whereas *Wcs* is slightly increased. $\varepsilon = \frac{1}{\mu\beta C}$ is inversely proportional to viscosity and the rheological parameters, β *and* C. Modification in these parameters clearly results in a significant change in Eyring-Powell fluid parameter, ε. *The reverse trend is induced with an increase in* $\delta = \frac{v^2}{2c^2x^2}$. For greater values of δ, the C_f and *Nu* are enhanced whereas *Wcs* is slightly decreased. An increase in *Pr*, manifests in a suppression in skin friction, C_f at the cone surface whereas it considerably increases wall couple stress, *Wcs* and Nusselt number, *Nu*. Prandtl number expresses the relative rate of momentum diffusion and thermal diffusion. If *Pr* > 1 then momentum diffusion rate exceeds thermal diffusion rate whereas if *Pr* < 1, the thermal diffusion rate exceeds the momentum diffusion rate. Prandtl number is also inversely proportional to thermal conductivity of the polymer (for fixed values of dynamic viscosity and specific heat capacity). Temperatures in the boundary layer are suppressed with greater Prandtl numbers (lower thermal conductivity of the polymer liquid). This enhances thermal diffusion to the wall (cone surface) which results in a boost in heat transfer rate to the wall i.e. increasing Nusselt numbers. There are many coupling terms between the temperature and the linear velocity, in Eqn. (9). In turn the linear momentum eqn (7) is coupled to the angular momentum eqn. (8) via several terms e.g. $\frac{n+7}{4} f g', \frac{1-n}{4}\xi\left(f'\frac{\partial g}{\partial \xi} - g'\frac{\partial f}{\partial \xi}\right)$ and this results in an indirect influence of the temperature

field on the micro-rotation field and therefore the wall couple stress. Similar observations have been made in Shamshuddin *et al.* [32] and Mishra *et al.* [33].

Fig. 2(a) - 2(c) illustrate the variations of velocity (f'), angular velocity (g) and temperature (θ) distributions with increasing *Eyring-Powell fluid parameter*, ε. Marked decreases in micro-rotation i.e. angular velocity (g) (Fig. 2b) is induced throughout the boundary layer transverse to the cone surface (i.e. with transverse coordinate, η = 0) with greater values of ε *since viscosity characteristics are modified in the polymer with this parameter*. Micro-rotation boundary layer thickness is therefore reduced with greater values of *Eyring-Powell fluid parameter,* ε. However, the linear velocity (f') (Fig. 2a) is initially enhanced near the cone surface (acceleration) and further from the wall a *strong deceleration* is induced which is sustained into the free stream. Temperatures are weakly increased with higher ε, implying a depletion in thermal boundary layer thickness. As $\varepsilon \to 0$ and $\delta \to 0$, the Eyring-Powell fluid model retracts to the classical Navier-Stokes (*Newtonian) flow model*. The micropolar parameter in Figs 3a-c, is constrained as K = 3 which implies strong concentrations of micro-elements (vortex viscosity is three times the Newtonian viscosity) and B = 0.5 implies relative large values of micro-inertia density parameter.

Fig. 3(a) – 3(c) visualize the impact of the *local non-Newtonian* parameter, δ on velocity (f'), angular velocity (g) and temperature (θ) distributions in the flow regime. A significant deceleration is induced in linear velocity (Fig. 3a) with increasing values of δ. This response is sustained throughout the boundary layer transverse to the cone surface. Hence the momentum boundary layer thickness is substantially increased. Similarly, a strong depression in temperature (Fig. 3b) is induced with increasing *local non-Newtonian* parameter, δ. The parameter δ appears solely in the linear momentum Eqn. (7), as the term, $-\varepsilon\delta(f'')^2 f'''$ and this acts as an opposing body force leading to inhibition of momentum diffusion (and via coupling with the energy eqn. (9) also impedes thermal diffusion). The contrary effect is generated however in the micro-rotation field (Fig. 3c) is instigated with increasing values of δ. The micro-elements are enhanced in their rotary motions (spin) and consistently the micro-rotation magnitudes are boosted at all values of transverse coordinate, η. It is also noteworthy that in all the figures plotted, asymptotically smooth profiles are achieved in the free stream (maximum η) confirming the prescription of an adequately large infinity boundary condition in the Keller box code.

Fig. 4(a) – 4(c) illustrate the evolution in linear velocity (f'), angular velocity i.e. micro-rotation (g) and temperature (θ) with a variation in *surface temperature exponent*, n. From **figs. 4a - 4c**, a significant decrease in linear (Fig. 4a) and angular velocity (Fig. 4b) and temperature is observed with an increase in the values of n throughout the boundary layer regime. The surface temperature exponent, n, simulates nonlinear variation in cone surface i.e. wall temperature. For $n > 0$ (temperature growth), an increase in wall temperature is observed along the cone surface and a decrease is induced for $n < 0$ (temperature decay). Attention is restricted to positive values of surface temperature exponent since these are more applicable in real thermal coating systems [1-3]. For $n = 0$ the wall is isothermal. As noted earlier the higher wall temperature achieved with non-isothermal behaviour reduces temperatures in the boundary layer (polymer). This decreases thermal boundary layer thickness and via coupling also leads to thicker momentum and thinner angular momentum boundary layers.

Fig. 5(a) – 5(c) illustrates the profiles for velocity (f'), angular velocity (g) and temperature (θ) distributions with a variation in the *micropolar vortex viscosity parameter* (K). For $K = 1$, the Newtonian fluid viscosity and micropolar vortex viscosity (due to micro-element spin) are equal. With $K = 0$, the micropolar effect is neglected and the non-polar form (Newtonian) case is retrieved. Inspection of fig. 5(a), shows that a strong acceleration is generated near the cone surface in linear velocity with increasing K values. Stronger vortex viscosity therefore accelerates the flow near the cone surface. However further from the cone surface the opposite effect is then induced and substantial deceleration in the flow is observed with greater vortex viscosity parameter. The agglomeration of micro-elements near the cone surface may contribute to the enhancement in linear velocity there. However, this effect will decay further from the wall and this may be the cause for the observed deceleration closer to the free stream. Temperature magnitudes are consistently enhanced throughout the boundary layer (Fig. 5b) with elevation in vortex viscosity values, K. Temperatures are therefore minimized for the Newtonian case (K=0) indicating that strongest cooling within the body of the polymer liquid corresponds to vanishing micropolar effect. Thermal boundary layer thickness is also enhanced with stronger vortex viscosity effect. Fig. 5(c) illustrates that significant elevation in micro-rotation is produced with increasing K values. The intensity of gyratory motions of micro-elements is clearly boosted with stronger micropolar vortex viscosity and this response is maintained throughout the boundary layer for all values of transverse coordinate. Angular (microrotation) boundary layer thickness is therefore elevated

with higher K values. The computations concur with earlier investigations including Ibrahim [31] and Latiff *et al.* [34]. Evidently the inclusion of micropolar effects yields significant deviation from Newtonian models. Neglection of micropolar rheological characteristics in the mathematical model developed for conical body polymer thermal coating flow would therefore under-predict temperatures and also under-predict linear velocities near the cone surface, in addition to completely ignoring micro-rotation characteristics of suspended particles in the polymer .

Fig. 6(a) – 6(c) shows the effects of the streamwise coordinate ξ on velocity (f'), angular velocity (g) and temperature (θ) distributions. The parameter ξ also features a local Grashof number, Gr_x and may be viewed in boundary layer simulation as a *free convection parameter*. Fig. 6(a) demonstrates that a considerable deceleration in the boundary layer flow is produced with greater values of ξ i.e. the flow is retarded with progression from the cone from the apex along the cone slant surface. The larger streamwise coordinate values correspond to a boost in thermal buoyancy forces and these supress the momentum momentum diffusion manifesting in polymer flow deceleration and a thicker momentum boundary layer. The deceleration is sustained for *all values* of streamwise coordinate. Maximum velocity is associated with the vertex on the cone i.e. $\xi = 0$. Fig. 6(b) shows that with increasing ξ values, there is a substantial decay in temperatures. Significant cooling is generated within the polymer and there is an associated depletion in thermal boundary layer thickness. Stronger free convection effect therefore is inhibitive to thermal diffusion in the polymer. Generally, a noticeable acceleration is induced in micro-rotation i.e. angular velocity (fig. 6(c)) is markedly elevated with larger values of streamwise coordinate, ξ. With progression along the cone surface from the vertex to the wider base, i.e. with larger values of ξ, the micro-elements are provided with increasing space in which to rotate and this serves to elevate angular velocity magnitudes. Micro-rotation values are maximum some distance transverse to the cone surface and as expected, in accordance with the boundary conditions (10) decay towards the free stream.

5.CONCLUSIONS

In this article, the Eyring-Powell micropolar fluid boundary layer flow and heat transfer on an inverted non-isothermal cone has been studied theoretically as model for thermal coating polymer processes. Steady-state and incompressible behaviour are assumed. During coating, the polymer molecular chains relax and the deformation is irreversible. Non-

Newtonian behaviour is critical to coating performance. The governing partial differential conservation equations and wall and free stream boundary conditions are transformed from an (x,y) coordinate system into a dimensionless boundary value problem in a (ξ, η) coordinate system. The second order accurate, implicit Keller-Box finite difference method (FDM) is deployed for the numerical solution. Validation with earlier Newtonian non-isothermal non-polar solutions from the literature is conducted. Graphical and tabulated results are presented to study the variations of fluid velocity, micro-rotation (angular velocity), temperature, skin friction, wall couple stress and wall heat transfer rate (Nusselt number). The computations have shown that:

(i)With increasing values of the first Eyring-Powell parameter temperatures are elevated, micro-rotation is suppressed and velocities are enhanced near the cone surface but reduced further into the boundary layer.

(ii)With greater values of the second Eyring-Powell parameter (local rheological parameter) linear velocity is boosted (i.e. momentum boundary layer thickness increased), temperature and thermal boundary layer thickness are reduced and micro-rotation (angular velocity) values elevated.

(iii)An increase in non-isothermal power law index (cone surface temperature index) depletes velocities, temperatures and micro-rotations i.e. linear momentum boundary layer thickness is elevated whereas thermal and angular momentum boundary layer thicknesses are reduced.

(iv) Maximum temperatures, velocities and micro-rotation correspond to the isothermal case (vanishing surface temperature exponent).

(v)Increasing Eringen vortex viscosity parameter significantly enhances temperatures and also micro-rotations but only generates linear velocity enhancement near the cone surface.

(vi) With increasing values of streamwise coordinate i.e. free convection parameter, i.e. the flow is retarded with progression from the cone from the apex along the cone slant surface and momentum boundary layer thickness elevated. Also, temperatures and thermal boundary layer thickness is decreased. However strong enhancement in micro-rotation i.e. angular velocity is generated with larger values of streamwise coordinate.

(vii) An enhancement in surface temperature exponent results in a depletion in skin friction, Nusselt number and wall couple stress.

(viii)An increase in Eringen vortex viscosity parameter elevates skin friction and wall couple stress whereas it reduces the Nusselt number.

(ix) Using isothermal models leads to over-prediction of flow and thermal characteristics in polymer thermal processing and non-isothermal models are recommended for more accurate estimation of skin friction and heat transfer rates.

The present numerical simulations have neglected rotation of the cone (of relevance to spin-coating) and also mass transfer i.e. species diffusion [56]. These aspects will be explored in the future. Furthermore, more sophisticated viscoelastic models (e.g. FENE-P models [57]) may be examined and efforts in this direction are underway.

REFERENCES

[1] F. Fanicchia *et al.,* Effect of microstructural modifications on the corrosion resistance of $CoCrFeMo_{0.85}Ni$ compositionally complex alloy coatings, *Coatings,* 9(11), 695 (2019).
[2] Choi, S. C. *et al.* Formation of an adherent layer by DC plasma polymerization, *Polymer Surface Modification: Relevance to Adhesion,* 2, 527-538 (2000).
[3] Chida K. Sakaguchi S.Wagatsuma M., and KimuraT. High-speed coating of optical fibers with thermally curable silicon resin using a pressure die, *Electron Letters,* 18, 713-715 (1982).
[4] Gutoff, EB, Cohen, ED, Kheboian, GI, *Coating and Drying Defects: Troubleshooting Operating Problems*. Wiley-Inter-science, New York (2006).
[5] N. Ali, A. Zaman, O. Anwar Bég, T. Hayat, Mathematical model for isothermal wire-coating from a bath of Giesekus viscoelastic fluid, *Chem. Eng. Comm.* 203, 1336-1248 (2016).
[6] Kistler, SF, Schweizer, PM, *Liquid Film Coating: Scientific Principles and Their Technological Implications*. Chapman & Hall, New York (1997).
[7] R.I. Tanner, *Engineering Rheology*, Oxford Engineering Science Series, Oxford University Press, UK (2000).
[8] A. Romo-Uribe, Dynamics and viscoelastic behavior of waterborne acrylic polymer/silica nanocomposite coatings, *Progress in Organic Coatings,* 129, 125-132 (2019).
[9] P. Lan *et al.,* A phenomenological elevated temperature friction model for viscoelastic polymer coatings based on nanoindentation, *Tribology International,* 11, 299-307 (2018).
[10] Y. Greener and S. Middleman, Blade-coating of a viscoelastic fluid, *Polymer Engineering and Science,*14, 791-796 (1974).
[11] Z. Khan *et al.,* Steady flow and heat transfer analysis of Phan-Thein-Tanner fluid in double-layer optical fiber coating analysis with Slip Conditions, *Scientific Reports,*6:34593 (2016).
[12] Ch. RamReddy, P. Naveen, and D. Srinivasacharya, Effects of nonlinear Boussinesq approximation and double dispersion on free convective flow of an Ostwald-De Waele power-law fluid along an inclined plate under convective thermal condition, J. Nanofluids, 7, 1247–1257 (2018).
[13] O. Anwar Bég, A. Subba Rao, N. Nagendra, CH. Amanulla, M. Surya Narayana Reddy and A. Kadir, Numerical study of hydromagnetic non-Newtonian nanofluid transport phenomena from a horizontal cylinder with thermal slip: aerospace nanomaterial enrobing simulation, *J. Nanofluids,* Vol. 7, pp. 1–14 (2018).

[14] Tasawar Hayat, Taseer Muhammad, Ahmed Alsaedi, Impact of Cattaneo–Christov heat flux in three-dimensional flow of second grade fluid over a stretching surface, *Chinese Journal of Physics*, 55, 1242-1251 (2017).
[15] R. Mehmood, Rabil Tabassum, S. Kuharat, O. Anwar Bég and M. Babaie, Thermal slip in oblique radiative nano-polymer gel transport with temperature-dependent viscosity: solar collector nanomaterial coating manufacturing simulation, *Arabian J. Science and Engineering (Springer) (2018). https://doi.org/10.1007/s13369-018-3599-y (17 pages)*
[16] R. E. Powell and H. Eyring, Mechanisms for the relaxation theory of viscosity, *Nature*, vol. 154, no. 3909, 427-428 (1944).
[17] I. Khan, M. Qasim, and S. Shafie, Flow of an Erying-Powell fluid over a stretching sheet in presence of chemical reaction, *Thermal Science International Scientific Journal*, vol. 20, pp. 1903–1912 (2016).
[18] W. Ibrahim and G. Gadisa, Finite element method solution of boundary layer flow of Powell-Eyring nanofluid over a nonlinear stretching surface, *Journal of Applied Mathematics*, Volume 2019, Article ID 3472518, 16 pages (2019).
[19] H. Yoon and A.J. Ghajar, A note on the Powell-Eyring fluid model, *International Communications in Heat and Mass Transfer*, 14, 381-390 (1987).
[20] S. Alharbi, *et al.*, Entropy generation in MHD Eyring–Powell fluid flow over an unsteady oscillatory porous stretching surface under the impact of thermal radiation and heat source/sink, *Applied Sciences*, vol. 8, no. 12, article 2588 (2018).
[21] M. Y. Malik, Imad Khan, Arif Hussain, and T. Salahuddin, Mixed convection flow of MHD Eyring-Powell nanofluid over a stretching sheet: A numerical study, *AIP Advances*, 5, 117118 (2015).
[22] V. Sirohi, M. G. Timol, and N. L. Kalthia, Powell-Eyring model flow near an accelerated plate, *Fluid Dynamics Research*, vol. 2, no. 3, pp. 193–204 (1987).
[23] J. Rahimi, D.D. Ganji, M. Khaki, Kh. Hosseinzadeh, Solution of the boundary layer flow of an Eyring-Powell non-Newtonian fluid over a linear stretching sheet by collocation method, *Alexandria Engineering Journal*, 2016, https://doi.org/10.1016/j.aej.2016.11.006
[24] S. Hina, M. Mustafa, T. Hayat, A. Alsaedi, Peristaltic transport of Powell–Eyring fluid in a curved channel with heat/mass transfer and wall properties, *International Journal of Heat and Mass Transfer*, 101,.156-165, (2016).
[25]I. Khan, Mair Khan, M.Y. Malik, T. Salahuddin, Shafquatullah, Mixed convection flow of Eyring-Powell nanofluid over a cone and plate with chemical reactive species, *Results in Physics*, 7, 3716-3722 (2017).
[26] Eringen, A.C., Simple microfluids, *Int. J. Engineering Science*, 2, 205-217 (1964).
[27] A.C. Eringen, Theory of micropolar fluids, *J. Mathematics Mechanics* 16 (1966) 1–18.
[28] A.C. Eringen, Theory of thermo-micropolar fluids, *J. Mathematical Analysis Applications*, 38 (1972) 480–496.
[29] N. Mohd. Arffin, N. Md. Arifin and N. Bachok, Marangoni boundary layer flow in micropolar fluid with suction/injection, *AIP Conference Proceedings*, Vol. 1795, Issue 1, 020011, 2017. https://doi.org/10.1063/1.4972155.
[30] N. Ali, Z. Asghar and O. Anwar Bég, A mathematical model of bacterial gliding on a thin layer of micropolar slime, *Results in Physics*, 9, 682-691 (2018).
[31] Ibrahim W, MHD boundary layer flow and heat transfer of micropolar fluid past a stretching sheet with second order slip, *J. Braz. Soc. Mech. Sci. Eng*., Vol. 39, Issue 3, pp. 791-799, 2017.
[32] Shamshuddin MD, Siva Reddy Sheri and O Anwar Bég, Oscillatory dissipative conjugate heat and mass transfer in chemically reacting micropolar flow with wall couple stress: A finite element numerical study, *Proc IMechE Part E: J Process Mechanical Engineering (2017).* DOI: 10.1177/0954408917743372 (17 pages)

[33] S. R. Mishra, I. Khan, Q. M. Al-Mdallal, T. Asifa, Free convection micropolar fluid flow and heat transfer over a shrinking sheet with heat source, *Case Studies in Thermal Engineering*, Vol. 11, pp.113-119, 2018.
[34] Nur Amalina Latiff, Md. Jashim Uddin, O. Anwar Bég and Ahmad Izani Md. Ismail, Unsteady forced bioconvection slip flow of a micropolar nanofluid from a stretching/ shrinking sheet, *Proc. IMECHE- Part N: J. Nanoengineering and Nanosystems,* 230 (4) pp. 177–187 (2016).
[35] H. Sobhani *et al.,* Non-isothermal modeling of a non-Newtonian fluid flow in a twin-screw extruder using the fictitious domain method, *Macromolecular Theory and Simulations*, 22, 462-474 (2013).
[36] X.K. Li *et al.,* Modelling of non-isothermal non-Newtonian viscoelastic flows, *Computational Mechanics*, ISCM2007, July 30-August 1, Beijing, China (2007).
[37] B. Debbaut, Non-isothermal and viscoelastic effects in the squeeze flow between infinite plates, *Journal of Non-Newtonian Fluid Mechanics,* 98, 15-31 (2001).
[38] G. Janardhana Reddy, Mahesh Kumar and O. Anwar Bég, Effect of temperature dependent viscosity on entropy generation in transient viscoelastic polymeric fluid flow from an isothermal vertical plate, *Physica A - Statistical Mechanics and its Applications*, 510, 426–445 (2018).
[39] B. Reisfeld and S.G. Bankoff, Non-isothermal flow of a liquid film on a horizontal cylinder, *J. Fluid Mechanics*, 236, 167-196 (1992).
[40] S. A.Gaffar, V. R. Prasad, B. Vijaya and O. Anwar Bég, Mixed convection flow of magnetic viscoelastic polymer from a non-isothermal wedge with Biot number effects, *Int. J. Engineering Mathematics,* Volume 2015, Article ID 287623, 15 pages (2015).
[41] F.B. Cheung, Analysis of freeze coating on a nonisothermal moving plate by a perturbation method, ASME *J. Heat Transfer*. 107(3): 549-556 (1985).
[42] M.M. Rashidi, O. Anwar Bég and M.T. Rastegari, A study of non-Newtonian flow and heat transfer over a non-isothermal wedge using the Homotopy Analysis Method, *Chemical Engineering Communications,* 199:2, 231-256 (2012).
[43] S.T.W. Kuruneru *et al.,* Transient heat transfer and non-isothermal particle-laden gas flows through porous metal foams of differing structure, *Applied Thermal Engineering, 150,* 888-903 (2019).
[44] O. Anwar Bég, M. Ferdows, Shamima Islam and M. Nazrul Islam, Numerical simulation of Marangoni magnetohydrodynamic bio-nanofluid convection from a non-isothermal surface with magnetic induction effects: a bio-nanomaterial manufacturing transport model, *J. Mechanics Medicine Biology*, 14, 3, 1450039.1-1450039.32 (32 pages) (2014).
[45] R.I.Nepershin, Non-isothermal plane plastic flow of a thin layer compressed by flat rigid dies, *International Journal of Mechanical Sciences, 39*, 899-912 (1997).
[46] Keller H.B., Numerical methods in boundary-layer theory, *Ann. Rev. Fluid Mech*. 10, 417-433 (1978).
[47] Hossain M.A., S. C. Paul, Free convection from a vertical permeable circular cone with non-uniform surface temperature, *Acta Mechanica,* 151, 103–114 (2001).
[48] S. Abdul Gaffar, V. Ramachandra Prasad, O. Anwar Bég, Md. H. Hidayathullah Khan and K. Venkatadri, Radiative and magnetohydrodynamics flow of third grade viscoelastic fluid past an isothermal inverted cone in the presence of heat generation/absorption, *J. Brazilian Soc. Mech Sci. Eng.,* 40:127-146 (2018).
[49] S. Ahmad *et al.,* Mixed convection boundary layer flow past an isothermal horizontal circular cylinder with temperature-dependent viscosity, *International Journal of Thermal Sciences,* 48, 1943-1948 (2009).
[50] S. Abdul Gaffar, V. Ramachandra Prasad, E. Keshava Reddy, O. Anwar Beg, Magnetohydrodynamic free convection boundary layer flow of non-Newtonian Tangent

Hyperbolic fluid from a vertical permeable cone with variable surface temperature, *J of Brazilian Society of Mechanical Sciences and Engineering*, 39, 101-116 (2017).
[51] K. Vajravelu *et al.,* Convective heat transfer in the flow of viscous Ag–water and Cu–water nanofluids over a stretching surface, *International Journal of Thermal Sciences*, 50, 843-851 (2011).
[52] O. Anwar Bég, V.R. Prasad, B. Vasu, Numerical study of mixed bioconvection in porous media saturated with nanofluid and containing oxytactic micro-organisms, *J. Mechanics Medicine Biology,* 13, 1350067.1-1350067.25 (2013).
[53] S. Siddiqa et al., Periodic magnetohydrodynamic natural convection flow of a micropolar fluid with radiation, *International Journal of Thermal Sciences*, 111, 215-222 (2017).
[54] S.A.Osman and T.A.M. Langlands, An implicit Keller Box numerical scheme for the solution of fractional sub-diffusion equations, *Applied Mathematics and Computation,* 348, 609-626 (2019).
[55] D. Incropera and D. DeWitt, *Fundamentals of Heat and Mass Transfer*, Wiley (1981).
[56] O. Anwar Bég, M.J. Uddin, Tasveer A. Bég, Ali Kadir, M Shamshuddin, M. Babaie. Modelling mass transfer from a rotating cone in anisotropic porous media with Stefan blowing and Navier slip, *Indian J. Physics* (2019) doi.org/10.1007/s12648-019-01520-9 (16 pages)
[57] M. Norouzi. S. Z. Daghighi. O. Anwar Bég Exact analysis of heat convection of viscoelastic FENE-P fluids through isothermal slits and tubes, *Meccanica,* 53, 817-831 (2018).